Spatial distribution of nonequilibrium electrons in quantum Hall devices: Imaging via cyclotron emission

Y. Kawano* and S. Komiyama
Department of Basic Science, University of Tokyo, Komaba 3-8-1, Meguro-ku, Tokyo 153-8902, Japan
(Received 15 December 2002; revised manuscript received 8 May 2003; published 29 August 2003)

Images of the spatial distribution of nonequilibrium electrons are studied in a wide quantum Hall effect (QHE) Hall bar ($\nu=2$) by detecting the local profile of the cyclotron radiation with an improved spatial resolution of 50 μm for the radiation wavelength of $\lambda=120$ μm. The experiments, along with conventional studies of voltage distribution via voltage probes, reveal the generation of nonequilibrium carriers at the diagonally opposite corners of Hall bars (hot spots) at low current levels (below 80 μA), as well as the occurrence of additional generation of nonequilibrium carriers at the corner opposite to the hot spot on the side of the source contact at higher currents (above 80 μA). The experimental findings are consistently interpreted in terms of earlier models of the electron dynamics around current contacts, providing support to the model of bootstrap-type electron heating for the breakdown of the QHE.

DOI: 10.1103/PhysRevB.68.085328 PACS number(s): 73.43.−f, 07.79.Fc

In the more than two decades since the discovery of quantum Hall effects (QHEs),[1,2] the role of metallic current contacts has not been fully understood. It is often suggested in the literature that the strong polarization fields concentrating at corners (hot spots) of the junction between metallic contacts and a two-dimensional electron gas (2DEG) layer in a Hall bar device[3] may cause the QHE to break down around current contacts. Surprisingly, however, an excellent quantization of the two-terminal (source-drain) resistance persists up to relatively large currents in a number of Hall bars,[4] the quantization being an apparent proof that the 2DEG layer, including the junction region, remains dissipationless. These seemingly conflicting features, as well as the influence of strong polarization fields on the dynamics of the electrons, should be clarified both from the basic viewpoint of better understanding QHEs and from the practical viewpoint of using QHEs for the resistance standard.[4]

Two effects should be considered in the junction region of metallic current contacts. One is the formation of a potential barrier at the junction and the tunneling of electrons to a 2DEG through the barrier.[5,6] The other is the influence of strong electric fields on the dynamics of electrons in the junction region.[7] These issues have been tackled experimentally by probing spatially resolved cyclotron emission.[6,7] The works lead to consistent models of current contacts, which accounted for the experimental findings. Unfortunately, however, the spatial resolution of the measurements was not necessarily sufficient to unambiguously establish the interpretation.

The purpose of this work is to shed more light on the issue by imaging nonequilibrium electrons in QHE Hall bars with higher resolution. To this end, we develop an improved scanning microscope system of far-infrared (FIR) radiation. When nonequilibrium electrons (holes) are excited in the Landau level above (below) the Fermi level, they emit a narrow-band cyclotron radiation upon the recombination process.[8,9] By locally detecting such extremely weak cyclotron radiation, this method visualizes the local density profile of nonequilibrium electrons (holes) excited in a 2DEG layer, which is inaccessible via resistance measurements. The improved spatial resolution as well as the improved sensitivity in this work makes it possible to reveal characteristic features of the local distribution of nonequilibrium electrons (holes), and provides strong support to the models proposed in Refs. 6 and 7.

According to geometrical optics, the diffraction limit of a microscope is given by $\delta=0.61\lambda/(n\sin\theta)$, where λ is the wavelength in vacuum, n the refractive index of a medium filling the space between an objective lens and an object, and θ the aperture angle. In our previous experiments with a remote objective lens ($n=1.0$, $\sin\theta=0.3$),[6,7] $\delta\approx300$ μm was obtained for $\lambda=120$ μm. Improvements are made by applying a solid immersion lens in the present work, as illustrated in Fig. 1(a). A hyperhemisphere lens with a 2.8-mm diameter and a 1.48-mm thickness, made of pure silicon crystal ($n_{Si}\approx3.4$), is in contact to the backside surface of the GaAs sample substrate ($n_{GaAs}\approx3.4$) of 0.5-mm thickness. The large refractive index of the media together with a large aperture angle, $\sin\theta=0.43$, predicts $\delta=48$ μm for $\lambda=120$ μm. Furthermore, collecting radiation on the back side of the GaAs substrate, along with the larger aperture angle, leads to an improvement of sensitivity by a factor roughly about 7.

The focal point of the lens is designed to be on the 2DEG layer embedded in the GaAs substrate at a 0.1-μm depth from the front surface. The cyclotron radiation emitted from the focal point is collimated via the lens, and is passed through a 30-mm-long and 1.7-mmϕ-bore black polyethylene pipe for filtering off-axis lights. The radiation is then guided through a 5-mmϕ-bore metal pipe to a highly sensitive wavelength-selective QHE detector[10,11] at a 29-cm distance. The sample and the detector are immersed in liquid helium, and placed, respectively, at the centers of two superconducting solenoids. The sample is mounted on a mechanical X-Y translation stage and moves relatively to the lens, so that its focal point scans the entire 2DEG area.

The sample is a Hall bar (the length $L=4$ mm and the width $W=1.5$ mm) fabricated on a GaAs/AlGaAs heterostructure crystal, as shown in Fig. 1 (b). The electron mobil-

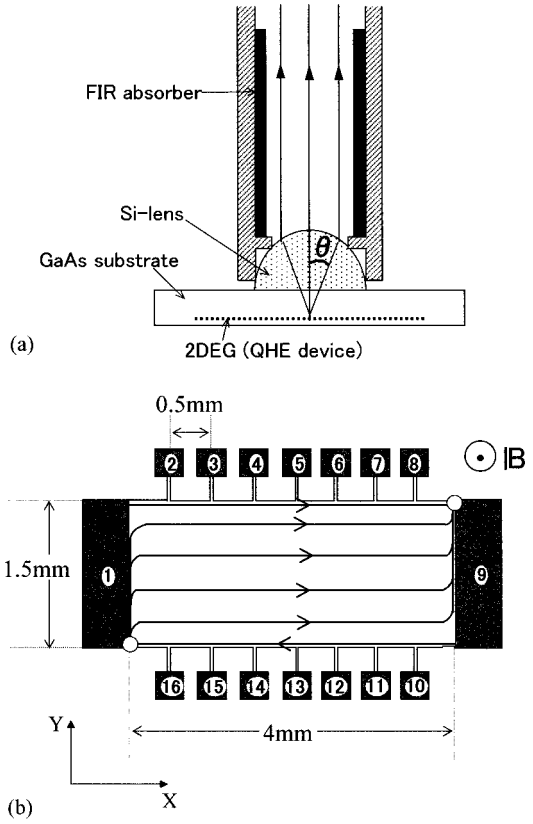

FIG. 1. (a) Optical scheme for detecting cyclotron radiation. The sample is mounted on an X-Y translation stage. (b) Schematics of the sample.

ity and the electron density are, respectively, $\mu=18$ m^2/Vs and $n_s=3\times10^{11}$ m^{-2} at 4.2 K. Eight pairs of voltage probes are placed at intervals of 0.5 mm. The arrows schematically represent electron trajectories in a magnetic field pointing out of the plane of the figure, and the white dots mark the diagonally opposite two hot spots. Rectangular-wave currents alternating between zero and a given finite value I at 30 Hz are passed through contacts 1 and 9, and the signal is recorded via a standard lock-in technique. The measurements are carried out at 4.2 K. Below contacts 1 and 9 serve, respectively, as the source and the drain of electrons ($V_1<0<V_9$) unless otherwise specified.

The resistances, $R_{91,91}=(V_9-V_1)/I$ and $R_{91,92}=(V_9-V_2)/I$, plotted in Fig. 2(a), show that the magnetic field of $B=6.1$ T corresponds to the QHE center at the filling factor of Landau levels, ν, equal to 2. Shown together is the FIR detector signal, V_{sig}, which shows the spatially integrated intensity of cyclotron emission (CE) at $I=70$ μA, where the magnetic field for the detector is chosen to be $B_D=6$ T. The resonant character of V_{sig} along with additional spectroscopic studies (not shown here) confirms that the detected radiation is the narrowband CE, and hence V_{sig} is a direct measure of the local density of nonequilibrium electrons (holes). For the studies below, the magnetic field is fixed at $B=6.1$ T ($\nu=2$), which yields a CE of $\lambda=120$ μm. Figure 2(b) compares the profiles of the CE intensity obtained in the present optical scheme (II) with those

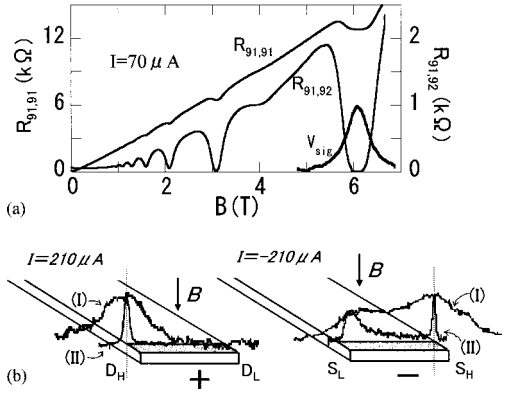

FIG. 2. (a) Two-terminal resistance $R_{91,91}$, three-terminal resistance $R_{91,92}$, and the CE signal V_{sig} against magnetic field B at $I=70$ μA. (b) Left and right panels display, respectively, the intensity profiles of the CE along junction regions of the drain contact (+) and the source contact (−), where the curves (I) taken with the earlier setup (Refs. 6 and 7) are compared with the curves (II) taken in the present optical scheme. For clarity, the signal intensities at the hot spots are normalized.

studied in the earlier free-space optic scheme (I),[6,7] where the left and the right panels display, respectively, the junction regions of the drain and the source contacts. The resolution is evidently improved, to a value $\delta\approx50$ μm close to the expected diffraction limit.

Figure 3 displays two-dimensional plots of the CE intensity at three different levels of current I. Shown together on both sides of each plot is the voltage distribution studied by using voltage probes: Voltage values of probe k, measured with respect to the drain contact 9, V_{9k}, are indicated at the X positions of the relevant probes, where the quantized Hall voltage is subtracted, V_{9k}-$(h/2e^2)I$, for the values on the right hand side ($k=2-8$) for clarity: On both sides, the value of V_{91}-$(h/2e^2)I$ is indicated at $X=0$ mm.

In this configuration, the electrochemical potential μ_S for electrons along the right-hand-side boundary, S_H-D_H, is higher than the one, μ_D, along the other boundary, S_L-D_L; μ_S-$\mu_D=(h/2e)I$. The corners S_L and D_H are the hot spots, at which Hall polarization fields are concentrated [Fig. 1(b)] and through which most of the electrons are injected into and withdrawn from the 2DEG layer. Additional measurements confirmed that all the features shown in Fig. 3 systematically change their spatial pattern upon the reversal of B and I, indicating that these features are of intrinsic physical origin.

We find that the two terminal resistance V_{91}/I remains quantized at $h/2e^2$ within an accuracy of 10^{-4} unless I exceeds 80 μA, the feature being consistent with earlier reports.[4,6,7] Despite the absence of dissipative longitudinal resistance, however, CE is visible in narrow regions around the electron entry-and-exit corners S_L and D_H, as shown in the top panel of Fig. 3 for $I=70$ μA, the feature confirming our earlier findings.[6]

As I exceeds 80 μA, there emerges a finite dissipative resistance in a limited region close to the source contact as shown in the middle and the lower panels of Fig. 3 for $I=250$ and 400 μA. In addition, additional CE develops in a region close to corner S_H that is opposite to the hot spot, S_L.

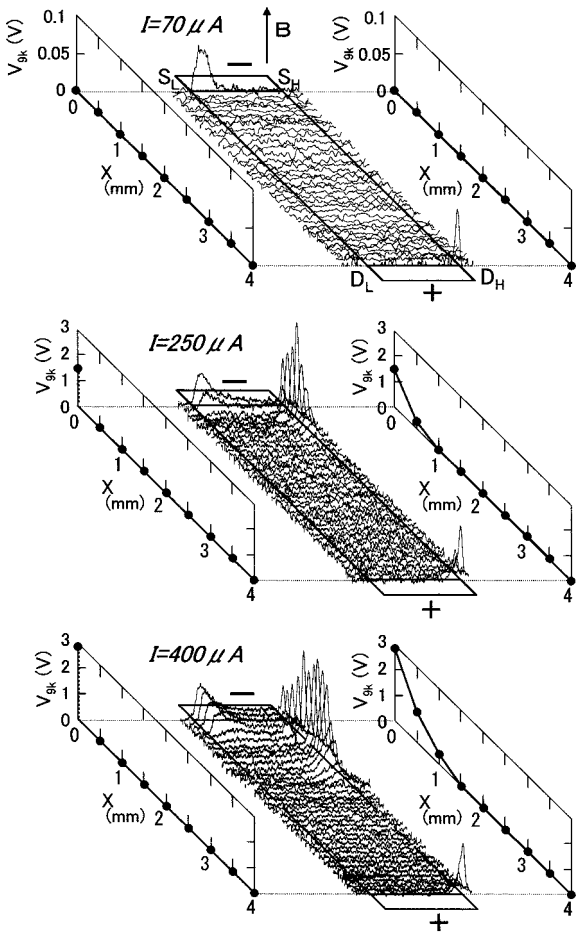

FIG. 3. Imaging plots of the CE. For clarity, the intensities at $I=70$ and 250 μA are magnified, respectively, by factors of 14 and 2 compared to that of $I=400$ μA. Voltage distribution along the opposite boundaries is displayed in the left- and right-hand panels.

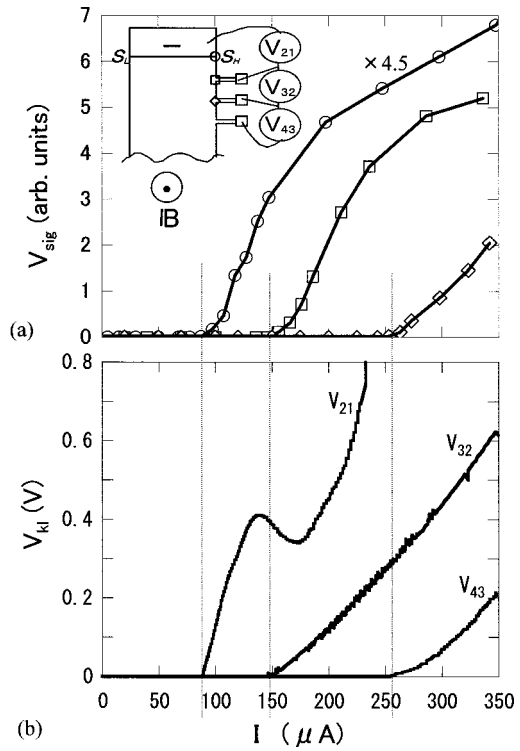

FIG. 4. (a) CE intensity V_{sig}, against I at three positions indicated in the inset by ○, □, and ◇. For clarity, the data (○) at S_H is magnified by a factor 4.5. (b) Voltages V_{21}, V_{32}, and V_{43} against I.

Distinct correlation between the additional CE and the voltage drop is confirmed by Fig. 4, where Fig. 4(a) plots the CE intensity V_{sig} as a function of I at three fixed positions; corner S_H (circles) and the joint corners of voltage probes 2 and 3 (squares and diamonds). The CEs are indiscernible at low current levels below 80 μA but increase abruptly, respectively, at $I=80$, 150, and 260 μA at these corners. Coincidence of the CEs with a finite voltage drop is demonstrated by the curves of V_{21}, V_{32}, and V_{43} versus I in Fig. 4(b). (We do not have a clear explanation for a small dip seen in the curve of V_{21} around $I=150$ μA.)

Profiles of the CE along boundary S_L-S_H ($Y=0$–1.5 mm) are displayed for different levels of I ($\geqslant 80$ μA) in Fig. 5(a). The bottom curve shows that CE is indiscernible along boundary S_L-S_H at $I=80$ μA, except the hot spot S_L ($Y=0$). As I increases, the CE peak at S_L ($Y=0$) increases its intensity, while additional CE rapidly grows, forming a more prominent, separated, peak at the opposite corner S_H ($Y=1.5$ mm). Another subtle but important feature is that, as I exceeds 80 μA, a weak but distinct background CE emerges along the entire boundary region. Two panels of Fig. 5(b) display CE profiles along boundary S_H-D_H ($X=0$–4 mm). The upper panel shows that the region of new CE is restricted to a narrow area around corner S_H ($X=0$) until $I=100$ μA is reached. The lower panel of Fig. 5(b) shows that, for $I>100$ μA, the region develops largely in the direction towards $X>0$, with a position of maximum intensity shifting away from corner S_H. (The curves for $I\geqslant 300$ μA are furnished with a peaked structure with a period about 0.2 mm, which is supposedly caused by an interference pattern of radiation and will not be discussed below.) In contrast, the region of CE on the side of drain contact is limited to the close vicinity of the hot spot, D_H, at all current levels.

The experimental findings in the above are consistent with, but give more detailed information than, the earlier data of lower-resolution CE experiments on Hall bars fabricated on a different GaAs/AlGaAs heterostructure crystal.[6,7] The CE found at corners S_L and D_H at lower current levels ($I\leqslant 80$ μA) is attributed to the generation of nonequilibrium electrons (holes) through tunneling across a potential barrier (fall) between the source (drain) contact and a 2DEG layer.[6] The absence of excess resistance up to $I=80$ μA, despite the generation of nonequilibrium carrier distribution around corners S_L and D_H, is readily understood by noting that voltage-probe contacts detect the electrochemical potential of edge channels.[12,13] Electrons in the edge channels along boundary S_H-D_H, with energies $\mu_S-(\hbar\omega_c)/2<\varepsilon<\mu_S$ with the Landau energy spacing $\hbar\omega_c=\hbar eB/m^*$, are supplied by the source contact (μ_S) at corner S_H and those along boundary S_L-D_L, with energies $\mu_D-(\hbar\omega_c)/2<\varepsilon<\mu_D$, by the drain contact ($\mu_D$) at corner D_L.[6] It follows that nonequi-

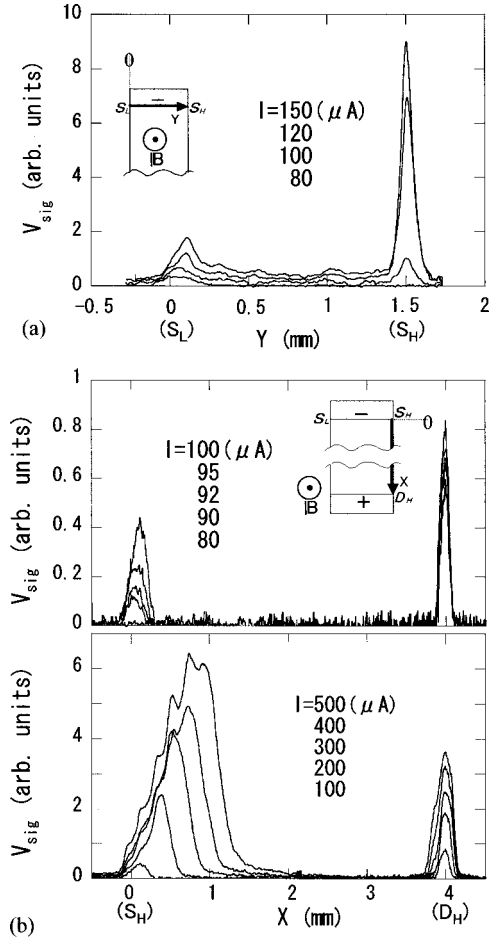

FIG. 5. Profiles of CE intensity at different currents: (a) Along the junction of the source contact, S_L-S_H, ($Y=0-1.5$ mm, $X=0$), the curves from the bottom ($I=80\ \mu$A) to the top ($I=150\ \mu$A). (b) Along the sample boundary, S_H-D_H, ($Y=1.5$ mm, $X=0-4$ mm). The current increases from the bottom curve to the top curve in respective panels.

librium carrier distribution around corner S_L or D_H does not affect the electron distribution in edge channels because these corners are, respectively, the ''down-stream'' terminals of the edge channels. The nonequilibrium carrier distribution along the junction region of the source contact also yields no detectable voltage drop unless it reaches corner S_H and affects the edge channel electron distribution.

Hence, the questions to be asked are (i) why CE is limited only to corners S_L and D_H up to $I=80\ \mu$A, and (ii) why an additional region of CE develops when $I>80\ \mu$A at corner S_H, and not in other regions. Our interpretation is deeply linked to the characteristics of the well-known current-induced breakdown of the QHE.[14–17] We note that the breakdown phenomenon is a relatively slow process of cascade-like multiplication of excited electron-hole pairs.[18–20] It is known in long Hall bars that the dissipative resistance R_{xx} increases abruptly when the average Hall electric field, $\langle E_H\rangle = V_{SD}/W$, in a 2DEG channel exceeds a critical value $E_c \approx 10^4$ V/m. On the other hand, the amplitude of polarization fields in the vicinity of corner S_L or D_H, roughly estimated as $E_{contact} \approx V_{SD}/l_B$ with $l_B=(\hbar/eB)^{1/2}$,[6,7] reaches $E_c \approx 10^4$ V/m already at a very small current level, $I \approx 10$ nA. Naively considered, therefore, the QHE would breakdown around corner S_L or D_H in most experimental conditions. However, the slow cascade process requires electrons to travel a sufficiently long distance before yielding appreciable resistivity.[18] Hence, electric fields higher than E_c have to be distributed over a macroscopic length along the trajectories followed by the electrons. The characteristic distance L_B needed for sufficient cascading is typically more than a few tens of micrometers at an electric field about 10% larger than E_c.[20,21]

On the side of the source contact, electrons with energies $\mu_D < \varepsilon < \mu_S - (\hbar\omega_c)/2$ are tunnel injected at corner S_L and drift along the junction S_L-S_H towards corner S_H.[5,6] If the longitudinal resistivity is strictly vanishing along the junction region, the polarization fields along this region are strong as well, with the highest amplitude at S_L and decreasing amplitudes along the junction towards S_H. Over a certain length range from corner S_L, the average field ${}^{av}E_{contact}$ may exceeds E_c. Electron-hole pair generation will take place in such a limited region where ${}^{av}E_{contact} > E_c$, yielding a finite resistivity. However, the induced finite resistivity, in turn, reduces the polarization fields. Hence, the polarization fields will be suppressed to a value close to E_c, and the electron-hole pair generation will be self-limiting to a minimal level.

The region of ${}^{av}E_{contact} > E_c$ may expand towards corner S_H as the current increases, but no appreciable CE may appear unless the region reaches corner S_H. We suppose that the region reaches S_H at $I=80\ \mu$A. At this stage, the self-consistent polarization fields over the entire region along S_L-S_H start to increase beyond E_c. This leads to a substantial distribution of nonequilibrium electrons (holes) along the junction that yields background CE along the entire junction region. At the same time, a strong peak of CE appears at the terminal of the cascade stream, corner S_H. As the current increases further, the region where ${}^{av}E > E_c$ expands further along boundary S_H-D_H, where the cascade generation continues to develop. The region of significant carrier generation is strongly weighted towards the higher potential boundary, S_H-D_H, at $I=400\ \mu$A (the bottom of Fig. 3). This feature might be explained by a theoretically expected nonuniform current distribution caused by an energy flux density that has a component pointing to higher potentials.[21]

On the other hand, the situation around the drain contact is different, as clearly seen in Fig. 5(b). On this side, the cascade generation of nonequilibrium carriers develops as the electrons move from corner D_L to D_H. A substantial nonequilibrium carrier distribution may build up at the terminal, corner D_H. However, this does not lead to a substantial intensification of CE at this corner, nor to an expansion of the CE region, because the nonequilibrium carriers reaching corner D_H are immediately absorbed by the drain contact.

Thus, all the experimental findings have been consistently interpreted. It may be worthwhile mentioning to Klaβ *et al.*'s experiments, where the spatial distribution of heat generation was studied in a Hall bar ($L=3$ mm, $W=2.5$ mm) with a 50-μm resolution.[22] Klaβ *et al.* found no signature of heat

generation except at the two hot spots (S_L and D_H) even with higher currents ($I>100$ μA). To interpret this discrepancy, we suggest that Klaβ *et al.*'s experiments probe the lattice temperature T_L, whereas the present experiments probe the effective electron temperature T_e. Furthermore, the present CE measurements are affected by the ratio of radiative recombination to the nonradiative process. In both experiments, the Hall resistance $R_H=12.9$ kΩ is substantially larger than the excess dissipative resistance (<8 kΩ), so that the heat generation $R_H I^2$ at the two hot spots (S_L, D_H) dominates the total dissipation. The heat generation around corners S_L and D_H is caused by electron tunneling, and is probably concentrated in narrow, spotlike regions, leading to an appreciable rise in T_L. However, the heat generation around a boundary region from S_H towards D_L, being caused by the dissipative resistance, may be more diffusive. On the other hand, we suppose that the probability of the radiative/nonradiative process is by more than one order of magnitude higher in the region outside the hot spots,[7] and this makes the CE visible outside the hot spots in the present experiments.

Finally, we note that the local breakdown of QHE around the source contact as discussed in this work occurs only in wide Hall bars ($W \gg L_B \approx 100$ μm) (Ref. 7): In narrower Hall bars ($W<100$ μm), the breakdown of the QHE develops in a region away from the source contact,[19] and strong polarization fields around current contacts do not have substantial effects on the breakdown characteristics.[7]

In summary, high-resolution images of the local density profile of nonequilibrium electrons in a wide QHE device have been studied through near-field imaging of cyclotron radiation. Breakdown of the QHE, induced by the presence of current contacts, is found to occur only when the current exceeds a critical value, where the region of breakdown is limited to the side of source contact, at a corner opposite to the hot spot. The experimental findings are consistent with the slowly developing character of the breakdown, which is predicted by the model of bootstrap-type electron heating.[18]

This work was supported by the Solution Oriented Research for Science and Technology (SORST) from Japan Science and Technology Corporation (JST) and by the Grant-in-Aid for Young Scientists (B) (14740185) from the Ministry of Education, Culture, Sports, Science and Technology, Japan.

*Present address: Department of Physics, University of Tokyo, Hongo 7-3-1, Bunkyou-ku, Tokyo 113-0033, Japan.

[1] K. v. Klitzing, G. Dorda, and M. Pepper, Phys. Rev. Lett. **45**, 494 (1980).

[2] S. Kawaji and J. Wakabayashi, in *Physics in High Magnetic Fields*, edited by S. Chikazumi and N. Miura (Springer, Berlin, 1981), p. 284.

[3] J. Wakabayashi and S. Kawaji, J. Phys. Soc. Jpn. **44**, 1839 (1978).

[4] As a review, see B. Jeckelmann and B. Jeanneret, Rep. Prog. Phys. **64**, 1603 (2001).

[5] P.C. van Son, G.H. Kruithof, and T.M. Klapwijk, Phys. Rev. B **42**, 11 267 (1990).

[6] Y. Kawano, Y. Hisanaga, and S. Komiyama, Phys. Rev. B **59**, 12 537 (1999).

[7] Y. Kawano and S. Komiyama, Phys. Rev. B **61**, 2931 (2000); Physica E (Amsterdam) **7**, 502 (2000); in *Proceedings of the 25th International Conference on Physics of Semiconductors (Osaka, 2000)* (Springer, Berlin, 2001), p. 921.

[8] See for instance, P.J. Burke, J.P. Eisenstein, L.N. Pfeiffer, and K.W. West, Rev. Sci. Instrum. **73**, 130 (2002), and references therein.

[9] K. von Klitzing *et al.*, in *Proceedings of the 17th International Conference on Physics of Semiconductors*, edited by J. D. Chadi and A. Harrison (Springer, New York, 1985), p. 271.

[10] Y. Kawano, Y. Hisanaga, H. Takenouchi, and S. Komiyama, J. Appl. Phys. **89**, 4037 (2001).

[11] See also, Y. Kawaguchi *et al.* Appl. Phys. Lett. **80**, 136 (2002); B.A. Andreev *et al.* Semicond. Sci. Technol. **16**, 300 (2001); N.G. Kalugin *et al.* Appl. Phys. Lett. **81**, 382 (2002).

[12] M. Bűttiker, Phys. Rev. B **38**, 9375 (1988).

[13] S. Komiyama and H. Hirai, Phys. Rev. B **40**, 7767 (1989).

[14] G. Ebert, K. von Klitzing, K. Ploog, and G. Weimann, J. Phys. C **16**, 5441 (1983).

[15] M.E. Cage *et al.*, Phys. Rev. Lett. **51**, 1374 (1983).

[16] S. Komiyama, T. Takamasu, S. Hiyamizu, and S. Sasa, Solid State Commun. **54**, 497 (1985).

[17] In our view, the fundamental physical mechanism of the QHE breakdown reported in Refs. 14–16 (also reported in much other literature) is the bootstrap-type electron heating discussed in Ref. 18. This mechanism is also common for the phenomenon discussed in this work.

[18] S. Komiyama and Y. Kawaguchi, Phys. Rev. B **61**, 2014 (2000).

[19] Y. Kawaguchi *et al.*, Jpn. J. Appl. Phys. **34**, 4309 (1995); Physica B **227**, 183 (1996); S. Komiyama, Y. Kawaguchi, T. Osada, and Y. Shiraki, Phys. Rev. Lett. **77**, 558 (1996).

[20] I.I. Kaya *et al.*, Phys. Rev. B **58**, R7536 (1998); Europhys. Lett. **46**, 62 (1999); Also see G. Nachtwei, Physica E (Amsterdam) **4**, 79 (1999).

[21] H. Akera, J. Phys. Soc. Jpn. **71**, 228 (2002).

[22] U. Klaß, W. Dietsche, K. von Klitzing, and K. Ploog, Z. Phys. B: Condens. Matter **82**, 351 (1991).